Stony Brook University

High-Flux Microfiltration Filters Based on Electrospun PVA Nanofibrous Mats

A Thesis Presented

by

Yang Liu

to

The Graduate School

in Partial Fulfillment of the

Requirements

for the Degree of

Master of Science

in

Chemistry

Stony Brook University

December 2009

Stony Brook University

The Graduate School

Yang Liu

We, the thesis committee for the above candidate for the
Master of Science degree, hereby recommend
acceptance of this thesis.

Benjamin Chu – Thesis Advisor
Distinguished Professor of Stony Brook University

Benjamin S. Hsiao – Thesis Advisor
Professor and Chair of the Chemistry Department

Stephen A. Koch – Chairperson of Defense
Professor of the Chemistry Department

Lisa Miller – Third Member
Adjunct Associate Professor of the Chemistry Department

This thesis is accepted by the Graduate School

Lawrence Martin
Dean of the Graduate School

Abstract of the Thesis

High-Flux Microfiltration Filters Based on Electrospun PVA Nanofibrous Mats

by

Yang Liu

Master of Science

in

Chemistry

Stony Brook University

2009

A novel class of high flux microfiltration membrane consisting of an electrospun nanofibrous membrane and a conventional non-woven microfibrous support is being presented. The nanofibrous membrane was fabricated by electrospinning of poly (vinyl alcohol) (PVA) followed by chemical cross-linking with glutaraldehyde (GA) in acetone. By altering the processing voltage and the concentration of PVA solution, electrospun PVA membranes with an average fiber diameter of 100 nm were obtained. Characterizations revealed that the mean pore size of the electrospun PVA membranes ranged from 0.32 μm to 0.21 μm with the membrane thickness varying from 10 μm to 100 μm. Due to the high porosity, these electrospun membranes showed 2.5 to 9 times higher pure water flux than the Millipore GSWP 0.22 μm membrane. The nanofibrous microfiltration membranes with a thickness of 20 μm could successfully reject more than

98% of the 0.2 μm polycarboxylate particles, and still be kept at a much higher permeate flux than that of the Millipore membrane. Therefore, this type of novel microfiltration media would be very useful in removing the bacteria for drinking water application. In addition, due to the high-filtration efficiency and low-cost fabrication of such filtration media, it could provide a potentially very important and promising pathway in solving the drinking water problem for many less developed countries in the world.

Table of Contents

List of Equations

List of Tables

List of Figures

Acknowledgements

I would like to express my deep gratitude and respect to my research advisors Professor Benjamin Chu and Professor Benjamin S. Hsiao for their invaluable advice, continuous patience, stimulating support and encouragement to my research. They are the ones I would admire and appreciate in all my life. Their strict attitude towards the scientific research deeply impressed me and will greatly influence my future career.

I would also like to give my thanks to my committee members, Professor Stephen A. Koch and Professor Lisa Miller for their help, suggestions and their encouragements on my way to the M.S. degree. Special thanks should also be given to the Student Affairs Coordinator of the Chemistry Department – Katherine M. Hughes, who I bothered most in the past two years, for her great help with numerous issues.

Many thanks to our current and previous group members Feng Zuo, Yimin Mao, Ran Wang, Xiaowei Li, Xiao Wang, Mahati Elluru, Kerin Wang, Shifeng Han, Lewis Yung, Nan Li, Drs. Dufei Fang, Hongyang Ma, Changquan Qiu, Christian Burger, Lixia Rong, Jie Zhu, Shigeyuki Toki, Jonathan Chiu, and Professor Chirakkal V. Krishnan. I thank them for their all kinds of help in research and daily life, as well as their helpful discussion in my thesis writing.

Finally, I would like to express my special appreciation to my parents and friends for their continuous understanding and support. I am also thankful for everyone that I have had in my life. Without them, I cannot go this far.

1. Introduction

1.1 Water scarcity

Clean, safe drinking water is the foundation of life and a basic human need. However, in the developing world, nearly 1 billion people do not have access to safe drinking water and almost 80% of illnesses can be linked to unsanitary water conditions. Worldwide, 1 out of every 4 deaths of children under the age of 5 is due to water-related diseases [1]. The limited availability of clean water has become a root cause of many problems in the world.

Drinking water can come from different resources, such as ground water and surface water. In some developing countries, where people cannot afford a pump to bring water from the ground, surface water often becomes the main source of daily drinking water. Due to high exposure to the environment, surface water from lakes and rivers usually contains fairly large amounts of bacteria, such as salmonella enterica, salmonella bacteria, Escherichia coli, vibrio cholera, sphingopyxis alaskensis [2]. As a result, water-borne diseases without proper purification are the source of a major health problem, especially in developing countries where, for example, 12.5 million people suffer from Typhoid fever every year, caused by the salmonella enterica from unpurified water. In Africa, about 125,000 cases of Cholera were reported in 2005, resulting from the vibrio cholera in drinking water. Other diseases in humans, such as the diarrhoeal disease, are also related with water borne bacteria. [3]

There are a number of organizations providing health care services as well as water

purification solutions in some African countries. For example, in Kenya the National Science Foundation has provided a method of straining water through a cloth, which can reduce certain amount of pathogens in the drinking water, including the bacterium that causes cholera[4]. Some companies are also aiming at designing devices which can filter out the bacteria from the surface water as it is being drunk, but they are usually too expensive for many people to afford such a scheme [5].

Table 1 Some commonly seen bacteria in water and their sizes [2]

Bacteria	Disease	Rod length/diameter (μm)
Salmonella enterica	Typhoid fever	2.0 - 5.0 / 0.7 - 1.5
Salmonella Bacteria	Salmonellosis	2.0 - 5.0 / 0.7-1.5
Pseudomonas aeruginosa	Otitis Externa	3.0 / 0.5 – 1.0
Escherichia coli	Colitis	2.0 – 4.0 / 0.8 – 1.0
Vibrio cholerae	Choloera	1.0 – 3.0 / 0.5 – 0.8
Yersinia enterocolitica	Yersiniosis	1.0 – 3.0 / 0.5 – 0.8
Listeria monocytogenes	Listeriosis	0.5 – 2.0 / 0.4 – 0.5
Mycobacterium marinum	M. marinum infection	1.0 - 4.0 / 0.25 - 0.6

While most of the water borne bacteria has a diameter of ≥ 0.3 microns, as listed in Table 1, it is possible to sterilize such contaminated water by filtration through membrane filters with pore size in the 0.2 micron size range. This method is capable of removing a substantial amount of the microorganisms (except viruses) from water and has been widely used in scientific research as well as medical and industrial applications [2-4]. However, when the method is applied to the purification of drinking water in daily

life in Africa, there are two major limitations. The first limitation is that the current commercial microfiltration membranes are too expensive; the second problem is that these commercially available microfiltration membranes exhibit very low throughputs at low pressures which makes it essentially impractical to purify drinking water effectively under less developed conditions where electrical power is essentially non-existent and sanitary conditions are minimal. Preparing microfiltration membranes with an average 'pore' size in the 0.2-0.3 micron length scale at low cost and with a sufficiently high flux at relatively low pressures will provide a potentially feasible pathway to help people in less developed countries to have access to save drinking water. It is the main objective of our study.

1.2 Microfiltration membrane

Membrane filtration technology has been improved dramatically over the past 30 years due to its cost-effectiveness, energy-efficiency and environmentally friendly operations [6, 7]. Ultra-filtration is currently playing a major role in pretreatment and purification of fresh water, brackish and saline water, as well as in waste-water treaatment [8, 9]. Classified by the pore size of membranes, the size and the charge of retained particles or molecules, and the pressure exerted on the membrane during the filtration process, filtration membranes can be distinguished as microfiltration (MF), ultrafiltration (UF), nanofiltration (NF), and reverse osmosis (RO) [10, 11], as listed in Table 2. Microfiltration membranes have the pore size ranging from 0.1 μm to 10 μm,

with the smallest pore sizes corresponding to the size of suspended solids, colloids. MF is an efficient process to remove bacteria and particle, and is often used as the pretreatment in water purification.

Table 2 Characteristics of different filtration membranes [10]

	Microfiltration (MF)	**Ultrafiltration (UF)**	**Nanofiltration (NF)**	**Reverse Osmosis (RO)**
Permeability ($L/h.m^2.bar$)	>1,000	10 - 1,000	1.5 - 30	0.05 - 1.5
Pressure (bar)	0.1 - 2	0.1 - 5	3 - 20	5 - 120
Pore size (nm)	100 - 10,000	2 - 100	0.5 - 2	< 0.5
Applications	Clarification; pretreatment; removal of bacteria	Removal of macromolecules, bacteria, viruses	Removal of (multivalent) ions and relatively small organics	Ultrapure water; desalination

Conventional microfiltration filters are based on porous membranes, typically manufactured by the phase immersion method [12] or phase inversion method [13-18]. The process induced by immersion precipitation is a well-known technique to prepare asymmetric membranes. By immersion, the solvent in the casting solution film is exchanged with non-solvent in the precipitation medium and phase separation occurs. This process results in an asymmetric membrane with a dense top layer and a porous sub-layer containing macro-voids, pores and micro-pores. The sub-layer formation is

controlled by numerous variables in the polymer dope solution, such as composition, coagulant temperature and organic/inorganic additives. Porous polymeric membranes manufactured by conventional methods have their intrinsic limitations, such as low-flux and high-fouling performance, due to the geometrical structure of pores, the corresponding pore size distribution and undesirable macro-void formation across the whole membrane thickness [19-23].

1.3 Electrospinning

Electrospinning is a process that produces continuous polymer fibers with diameters in the sub-micron size range through the action of an external applied electric field imposed on a spinneret containing polymer solution [24]. Charges are induced within the fluid when a high voltage is applied to the polymer solution [25]. When the charges reach a critical amount and the Columbic repulsion force overcomes the surface tension and the viscoelastic force of the solution, a fluid jet will erupt from the tip of the spinneret and forms the well-known “Taylor cone”. The jet travelling down towards the region of lower potential—collector in most cases becomes elongated and further thins down due to stretching and bending instabilities, which is caused by the repulsive force between charges in the jet. The process continues until solidification takes place with the dried or slightly damp nanofiber finally depositing on the collector [26-29]. Recently, Electrospinning has received a great deal of attention because it can produce nanometer diameter fibers easily from either natural [30] or synthetic [31] polymers, with widely

ranging applications in fields such as filtration [32], biomedical application [33], composites [34], fuel cells etc.

For electrospun membranes, the pores are caused by the entanglement of nanofibers and are fully interconnected. Therefore they usually exhibit good tensile strength and lightweight. The pore size is relatively small and the porosity is up to 70 % ~ 80 % or even higher, so the electrospun membranes should be particularly suitable for fluid filtration as the pores are not easily blocked by particles that penetrate into the filter. Our group [12, 20, 35] has successfully applied the electrospun membranes for ultrafiltration and nanofiltration.

A number of studies has addressed the relationship between the pore size and the electrospun nanofiber diameter, revealing that the smaller the fiber diameter, the smaller the average pore size [26, 36, 37]. For example, Kim and co-workers reported the physical properties of non-woven mats composed of nylon-6 nanofibers. Depending on the fiber diameter, the average pore size was in the range of 2.7~0.17 microns and the porosity varied from 25 % ~ 80 % [38]. Empirically, the average pore size is nearly 2~3 times of the fiber diameter from these studies. So it can be hypothesized that if the electrospun nanofiber diameter is lowered down to 100 nm, there will be a reasonably good chance that the average 'pore' size can be limited to around 0.3 μm.

In the electrospinning process, the fiber diameter is affected by many parameters either directly or indirectly. These parameters include properties of polymer solutions such as the solution viscosity, surface tension, solution conductivity, processing

conditions such as voltage, solution flow rate, distance between the spinneret tip and the collector [25]. Ambient parameters like humidity, temperature, pressure, type of atmosphere are also important to influence the fiber diameter [39-43]. Many mathematical models have been set up to try to illustrate the relationship between these parameters and the fiber diameter [29], but it is difficult to include all variables which are actually coupled with one another into one model. So up to now, control over the fiber diameter in electrospinning still remains a technical bottleneck and often requires empirical by adjusting the typical spinning parameters.

Poly (vinyl alcohol) (PVA) is chosen as the material for the electrospun membrane because it is an inexpensive material and is not degradable under most physiological conditions [35]. However, as PVA is a water-soluble polymer, it has to be treated with cross-linking reagents to form a three-dimensional water-resistant network [44, 45]. In this study, PVA nanofibers were successfully electrospun with the diameter of 100 nm by controlling the electrospinning conditions.

In another aspect, once a filtration membrane is formed, two key factors define its functionality: flux and selectivity [46], which are affected by properties such as the membrane thickness, porosity, and pore size. For microporous membranes, a single pore size value is not sufficient for characterization as the pores have to be assumed to have a size distribution [47]. Many methods have been used to determine the average pore size and the pore size distribution of microporous membranes, including mercury intrusion porosimetry, liquid extrusion porosimetry [48], electron microscopy, adsorption-base

methods and capillary flow porometry [37, 47, 48]. Among these, capillary flow porometry is a simple, fast, non-toxic and non-destructive technique that has been widely used in many commercially available automated equipment for membrane characterizations. In a capillary flow porometry measurement, a non-reacting gas (typically air or nitrogen) flows through a dry sample and then through the wet sample which has been wet with a liquid having a low surface tension and low vapor pressure. The flow rate is recorded as a function of pressure for both dry and wet processes. Pore size distribution as well as mean pore size can be derived from calculations.

In this study, cross-linked polyvinyl alcohol (PVA) electrospun membranes with different thicknesses were prepared. Membrane properties such as pure water flux, mean pore size and pore size distribution were investigated. To better understand the capability and performance of the membranes in removing bacteria, the rejection test using particles with an average diameter of 0.2 μm and a narrow size distribution was conducted. Certain properties of the commercial microfiltration membrane Millipore GSWP with a nominal pore size of 0.22 μm were also studied and compared with those of electrospun PVA membranes.

2. Experimental

2.1 Materials

Poly (vinyl alcohol) (PVA) with a weight-average molecular weight (M_w) of 75,000 g/mol was purchased from Kuraray Co. Ltd, Japan. Glutaraldehyde (GA) (50% aqueous solution), hydrochloric acid (36.5% aqueous solution) and acetone (99.8%) were obtained from Aldrich and used as received. Sodium chloride was purchased from Fisher Scientific. The non-woven polyethylene terephthalate (PET) with average fiber diameter of around 10 μm was purchased from Sanko Ltd, Japan, and was used as the substrate. Polycarboxylate microspheres with the diameter of 0.209 ± 0.011 μm used for the rejection test was purchased from Polysciences. Inc.

2.2 Preparation and characterization of PVA solutions

PVA was dissolved in distilled water at 90 °C and was stirred for 1 day to ensure homogeneity. Four different concentrations (6, 8, 10, 12 wt %) of PVA solutions were prepared to test the effects of solution concentration on the fiber diameter. Three different ratios of sodium chloride (0.1, 0.2, 0.5 wt %) were added to a PVA solution of specified concentration in order to investigate the effects of ionic salt addition on the electrospun fibers.

The viscosity of polymer solution was determined by using a Brookfield digital viscometer (model LVTDCP) at 24.0 °C. The electric conductivity was measured with the Oakton conductivity/TDS/°C meter (CON 11 Series).

2.3 Electrospinning of PVA nanofibrous membrane

A schematic diagram of the electrospinning device for fabricating fibers of small diameters is shown in Fig. 1. The power supplies from Glassman High Voltage, Inc were used to supply the applied voltage of 0-40 kV. Polymer solution was fed to the spinneret (diameter 1 mm) tip at controllable flow rates ranging from 5-100 μL/min, through a BD syringe using a syringe pump from Welmex Inc. The process was operated in a closed chamber, with the relative humidity controlled at 55% ± 5% and temperature at 24 °C ± 1 °C during the electrospinning process. An air drier and a humidifier were used to introduce dried or wet air in order to adjust the humidity of the chamber, and a heating tape from McMaster was placed on the back wall of the chamber to adjust the temperature when necessary. A temperature sensor and a humidity sensor manufactured by Fisher Scientific were used to monitor the temperature and the humidity in the chamber. A grounded metal drum (diameter: 10 cm) with a rotating speed of 300 rpm was used as the collector and was placed 10 cm below the tip of the spinneret. A stepping motor was used to control the oscillatory translational motion perpendicular to the drum rotation direction to ensure the production of uniform electrospun membrane with sufficient membrane area. The thickness of membranes was controlled by the volume of polymer solution delivered.

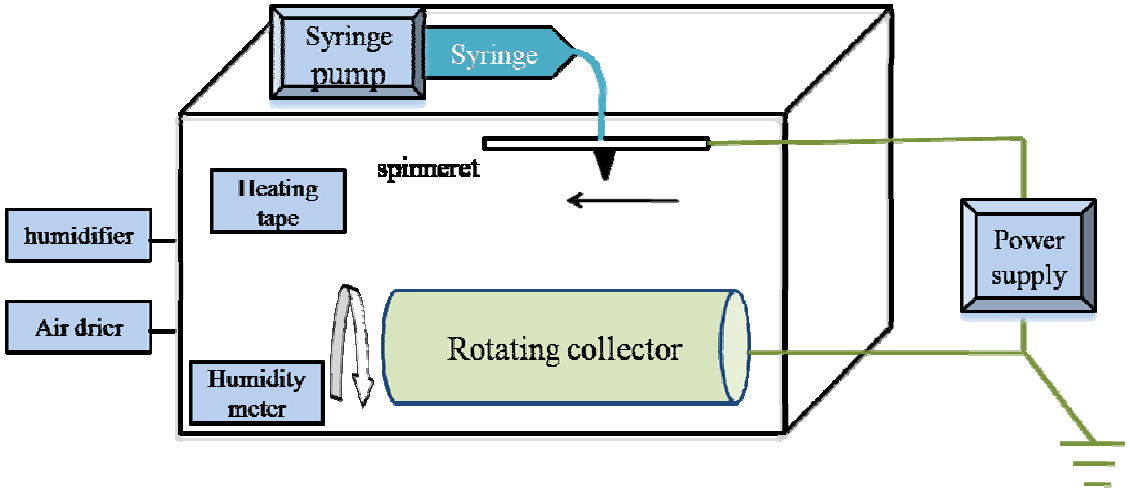

Figure 1 Schematic diagram of electrospinning setup

2.4 Cross-linking of electrospun PVA membrane

As electrospun PVA nanofibers can be dissolved in water, cross-linking of the electrospun PVA membrane has to be performed before use. PVA can be chemically cross-linked with many aldehydes, such as GA and glyoxal [49]. The reaction is due to the formation of acetal bridges between the hydroxyl groups in PVA and the aldehyde molecules, shown in Fig. 2. The cross-linking procedures are as follows. Electrospun PVA substrate was immersed in 0.15 M GA and 0.05 M HCl in acetone solution for 1 hour to ensure completion of the cross-linking reaction. The cross-linked PVA membrane was taken out and washed in water, and then dried in vacuum before use [35].

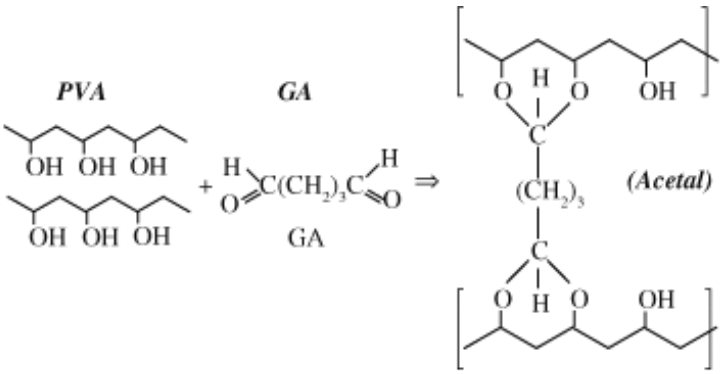

Figure 2 Cross-linking reaction of PVA with GA.

2.5 Characterization of fiber diameter

Electrospun fibers were imaged using a scanning electron microscope (SEM) (Phenom, FEI) after gold-sputter coating (SC7620 Sputter Coater, Quorum Technologies). Samples were coated at a current of 18 mA and under vacuum of 0.1 mbar for 30 seconds. The average diameter of the fibers was analyzed from the SEM images using the LeicaIMGRead software. At least four images were taken from different spots of each sample and 100 different fibers were used to calculate the fiber diameter. Results were reported as mean ± standard deviation.

2.6 Membrane characterizations

2.6.1 Thickness and porosity

The thickness and porosity of the electrospun PVA membrane were measured after peeling the PVA membrane from the PET substrate. The thickness was measured using a micrometer, and the porosity of the electrospun PVA membranes was calculated by using equation:

$$\text{porosity} = \left(1 - {}^{\rho}/_{\rho_0}\right) \times 100 \qquad (1)$$

where ρ is the density of electrospun membrane, determined from an average of four samples using mass divided by volume of the sample, and ρ_0 is the density of the PVA polymer.

.

2.6.2 *Pore size distribution*

The pore size distribution of the electrospun membranes was determined by capillary flow porometry. A schematic diagram of the capillary flow porometry set-up is shown in Fig. 3.

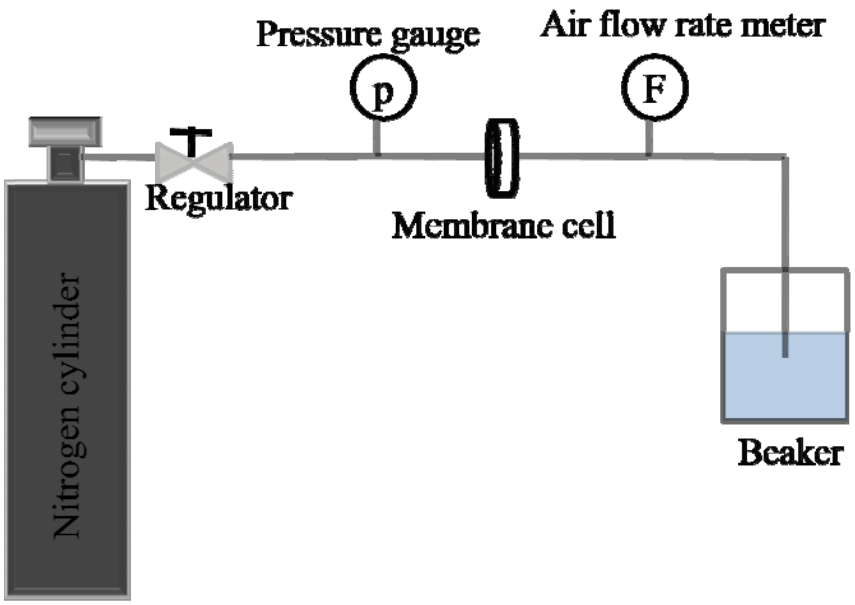

Figure 3 Schematic diagram of the pore size distribution test [46]

The membrane was placed in the membrane cell with a diameter of 25 mm. A wetting fluid, Porofil (QuantaPhi Corporation, US) with a surface tension of 15.9 dynes/cm was used to wet the membrane and to fill the pores spontaneously. The

differential pressure of nitrogen gas was applied and slowly increased on the membrane. Based on the Young-Laplace equation

$$D = \frac{4\gamma}{\Delta P}\cos\theta \qquad (2)$$

(where D is the maximum diameter of the pore, ΔP differential pressure, γ the surface tension of the wetting reagent, and θ is the wetting angle) and as the pressure was increased, the gas would reach a point where it could overcome the surface tension of the liquid in the largest pores and would push the liquid out. The first air bubble would be observed. The corresponding pressure that produces the first air bubble can be related to the maximum pore size of the membrane. The the flow rate was recorded with a Smart-Trak 2 digit mass flow meter (Sierra Instruments, US). With the pressure further increased, smaller pores would be open until the membrane became “dry” when all the pores were open. The relationship between the air flow rate and the differential pressure was plotted as the “wet curve”. The pressure and the air flow rate through a dry membrane were also measured and plotted as the “dry curve”. For determination of the mean pore size of the membrane, a “half-dry curve” that gives half of the flow rate through the dry membrane at a certain differential pressure was computed. The mean flow pressure was determined as the differential pressure corresponding to the intersection of the half-dry curve with the wet curve, and the mean pore size was calculated with Equation 2. The mean pore size is such that 50 % of the flow is through pores larger than the mean pore size and 50 % of the flow is through pores smaller than the mean pore size. The pore size distribution of the membrane was calculated from the

differential pressures and air flow rates by using equation [50]:

$$f = -d\left[\left(\frac{F_w}{F_d}\right) \times 100\right]/dD \qquad (3)$$

where f is the probability of the pore size with the diameter D. F_w and F_d are flow rates through the wet and dry membrane respectively.

Three runs were performed on each membrane to validate the precision of the measurements.

2.6.3 Pure water flux

The pure water flux of the electrospun membranes was studied by using a lab-built dead-end filtration set-up, as shown in Fig. 4 [46]. A water tank filled with distilled water was placed between the compressed nitrogen tank and the membrane cell. The driven pressure was measured using a digital pressure gauge and was kept at 2.3 ± 0.05 psi during the measurement.

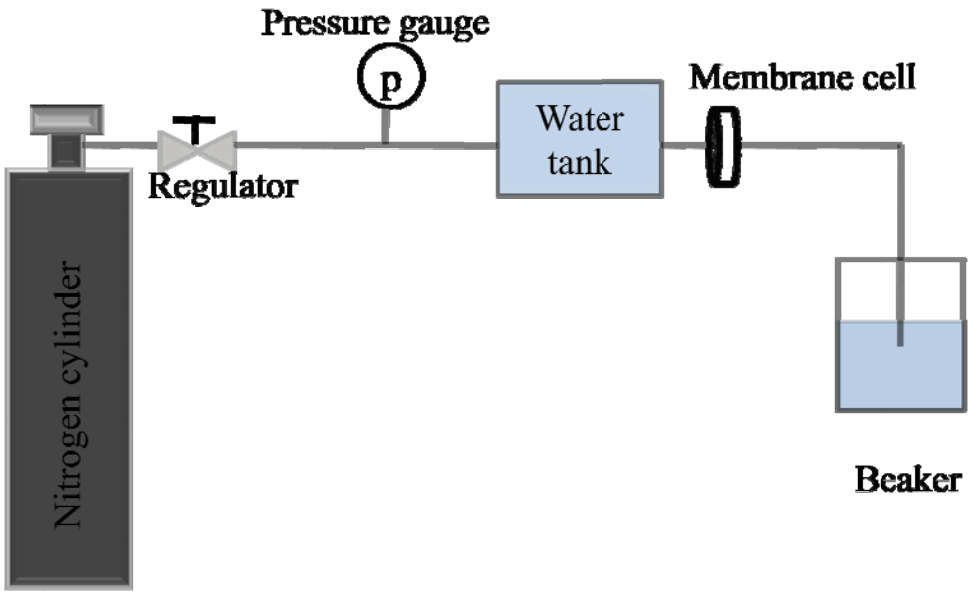

Figure 4 Schematic diagram of the lab-built dead-end filtration set-up [46]

2.6.4 Particle rejection test

Set-up of rejection test was achieved by simply replacing the pure water in the flux test by the polycarboxylate feed solution. A suspension of polycarboxylate particles with a diameter of 0.209 ± 0.011 μm was diluted in water to prepare a polycarboxylate particle suspension at a concentration of 250 ppm to serve as the feed solution. For each membrane, the rejection test was run for 20 minutes at the pressure of 5 psi, and the permeate was collected at 1st, 3rd, 5th, 10th and 20th minute. A total Organic Carbon Analyzer (TOC) (Shimadzu Corporation, Japan) was used to measure the concentrations of the feed solution and of the permeate and the rejection ratio was calculated using equation:

$$\text{rejection} = \left(1 - {C_{permeate}}/{C_{feed}}\right) \times 100 \qquad (4)$$

where $C_{permeate}$ and C_{feed} are the polycarboxylate concentration in the permeate and the feed.

3. Results and discussion

3.1 Electrospinning processing parameters

In this study, the PVA polymer solution was electrospun onto the PET non-woven substrate at the humidity of 55% ± 5% and temperature of 24 °C ± 1 °C. The following variables including solution properties (concentration and ionic salt addition) and processing parameters (applied electric field) have been examined. Their relationships

with the electrospun nanofiber diameter and the membrane porosity are summarized below.

3.1.1 Electric field effect

Electrospinning is a process involving various forces and properties of polymer solution, such as electrical force, surface tension and viscoelastic force of the solution, etc. We confirm that the morphology and the fiber diameter can be changed by increasing the voltage.

For the 8 wt% PVA solution at a flow rate of 10 μl/min, the morphologies of the membrane obtained under different accelerating voltages (24, 28, 32 kV) are shown in Fig. 5. It can be seen that at an applied voltage of 24 kV, the fiber morphology showed a great deal of beads or microdroplets with an average fiber diameter of 220 nm. At lower voltages, the Columbic repulsion could not overcome the surface tension and the viscoelastic force of the solution. As a result, the Taylor cone was not able to be formed in the jet initiation, which resulted in the observation of jet dripping and microdroplets formed in the structure. As increasing voltage, the beads in the structure became less and smaller in size, and the average fiber diameter was reduced to 140 nm at 28 kV and 100 nm at 32 kV. The decrease in the average fiber diameter could be attributed to the greater elongation force provided by the increase in the electric field strength.

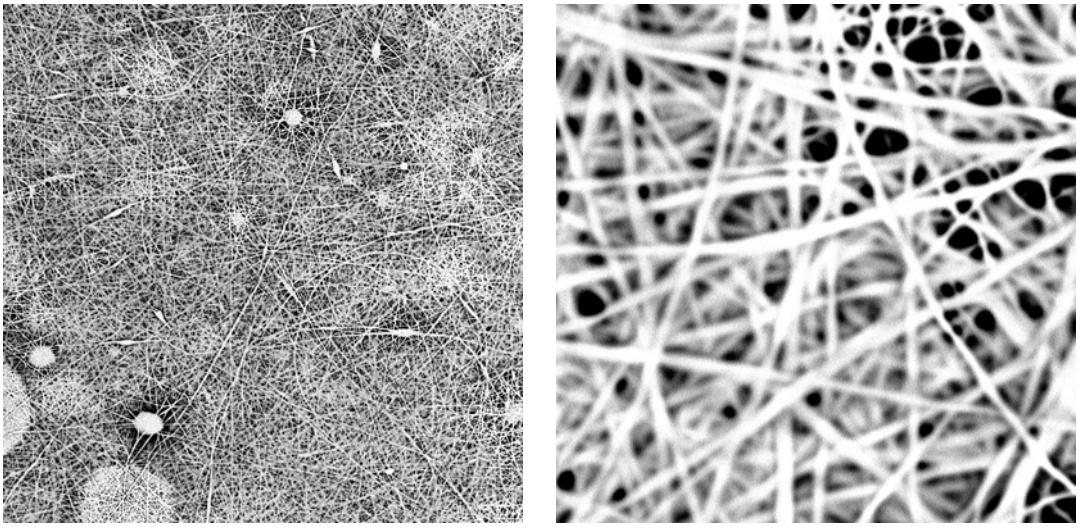

(a) 24 kV

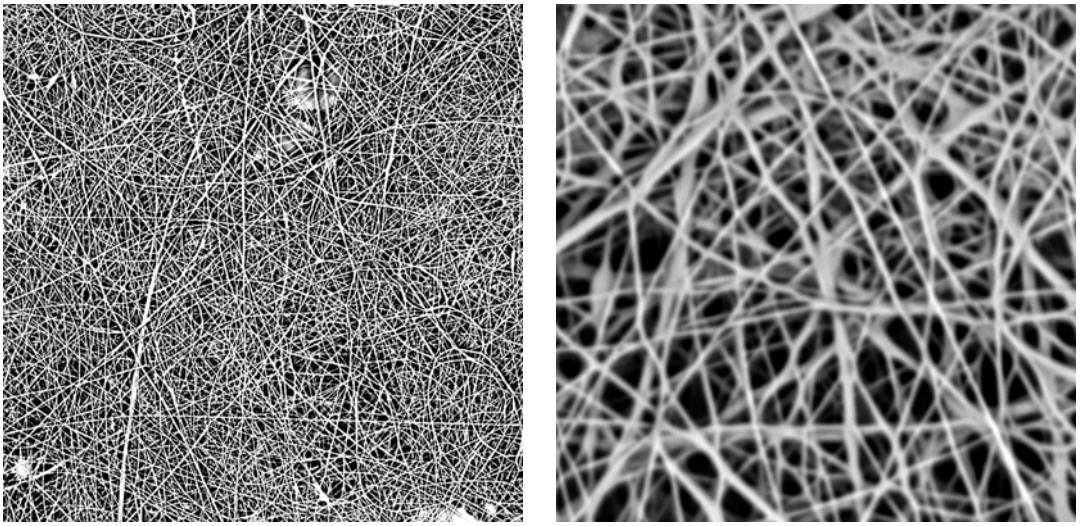

(b) 28 kV

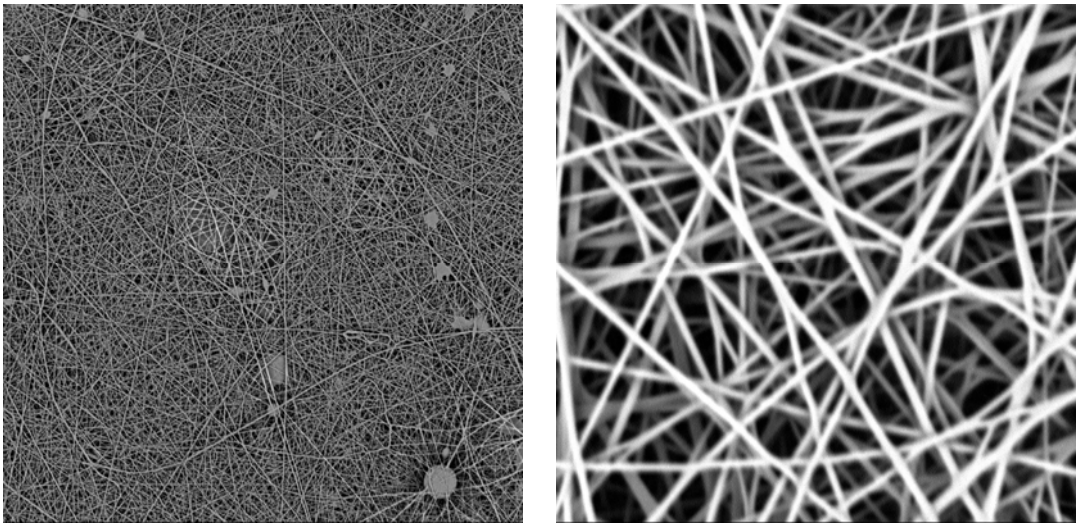

(c) 32kV

Figure 5 SEM images of PVA membranes fabricated on the PET non-woven substrate by electrospinning of an 8 wt% solution at a flow rate of 10 μL/min and the voltages of (a) 24 kV; (b) 28 kV; (C) 32 kV. Other electrospinning parameters: distance from spinneret to the collector: 10 cm; humidity 55% ± 5%; temperature 24 °C ± 1 °C.

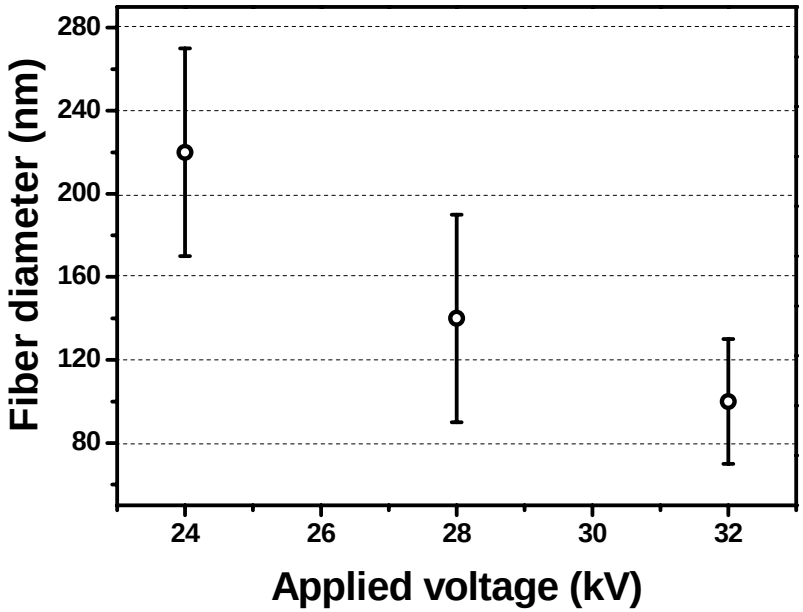

Figure 6 Effects of applied voltage on the diameter of electrospun PVA nanofibers fabricated from 8 wt% PVA solution. Flow rate was 10 μL/min.

3.1.2 Concentration effect

PVA solutions were prepared at various concentrations, ranging from 6% to 12%. Fig. 7 shows the viscosity of the PVA solution as a function of concentration. The viscosity values for PVA solutions were found to increase with increasing concentration. Specifically, there was a sharp increase of the viscosity from 50 cp to 669 cp when the concentration was increased from 10% to 12%. The relationship between the viscosity of PVA solution and the concentration could be estimated with an exponential growth equation (see equation in Fig. 7).

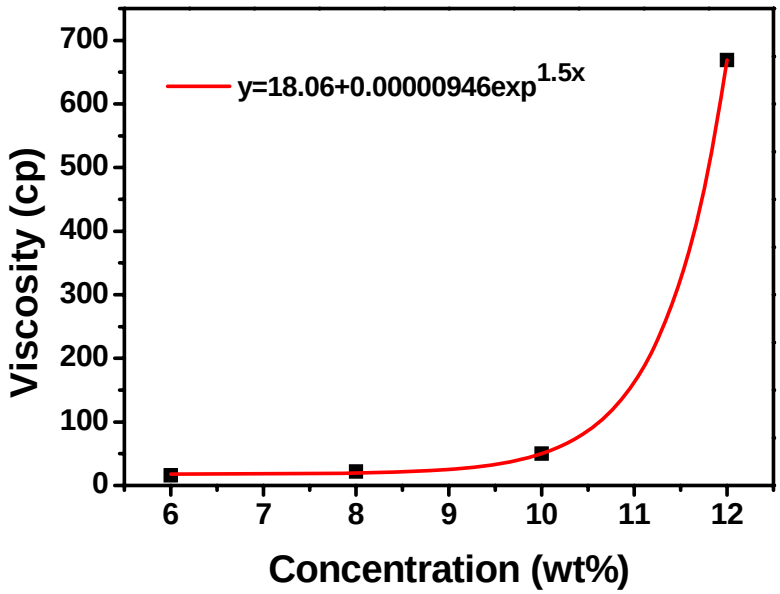

Figure 7 Viscosity as a function of concentration of PVA solutions.

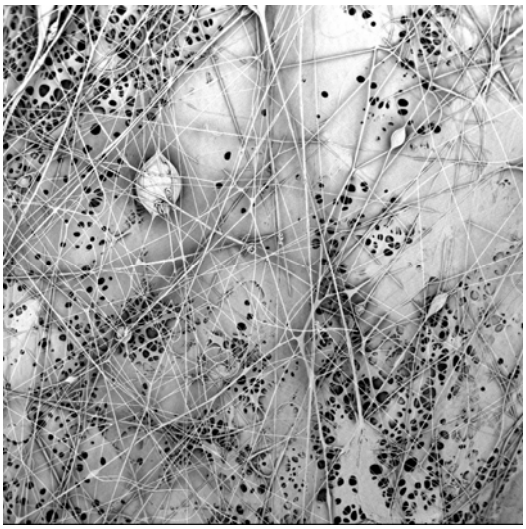

(a) 6%

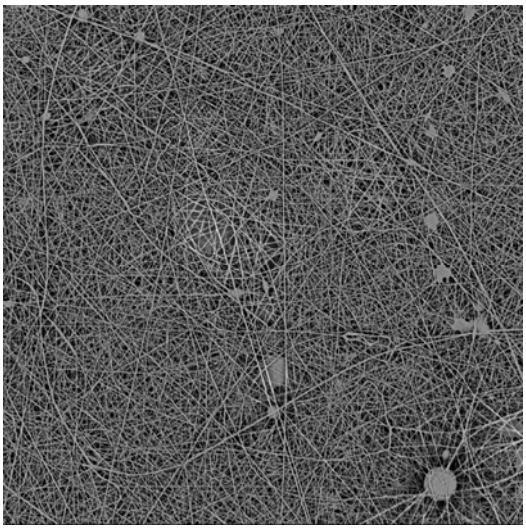

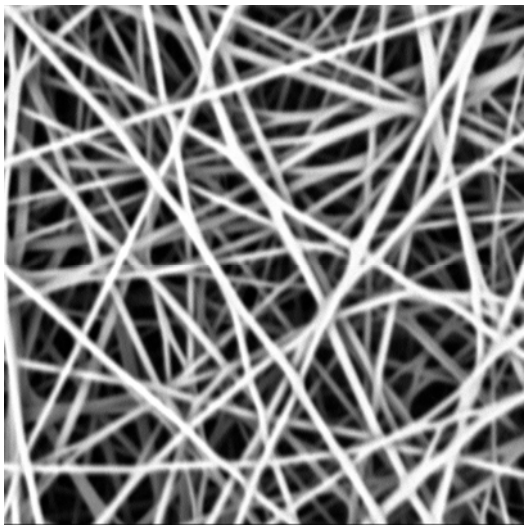

(b) 8%

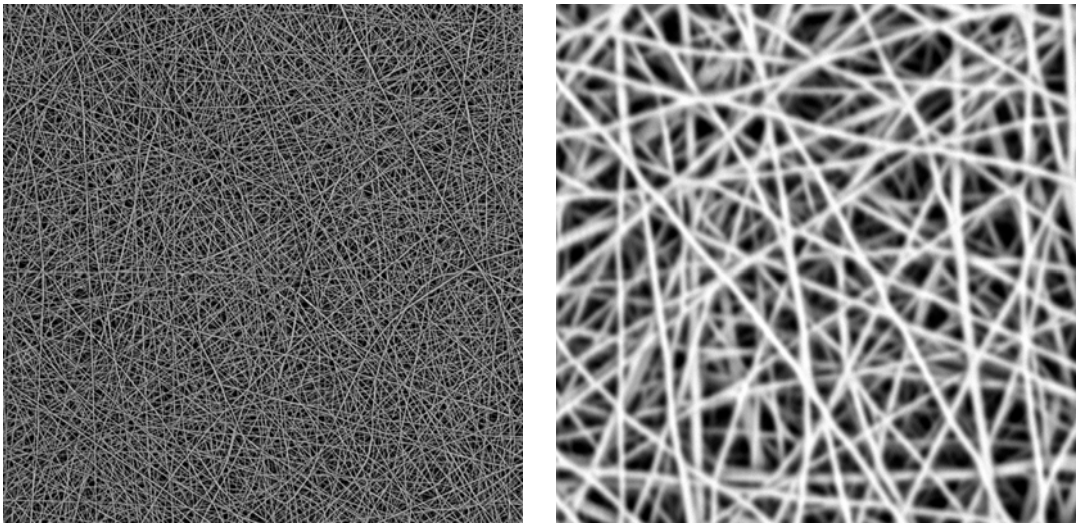

(c) 10%

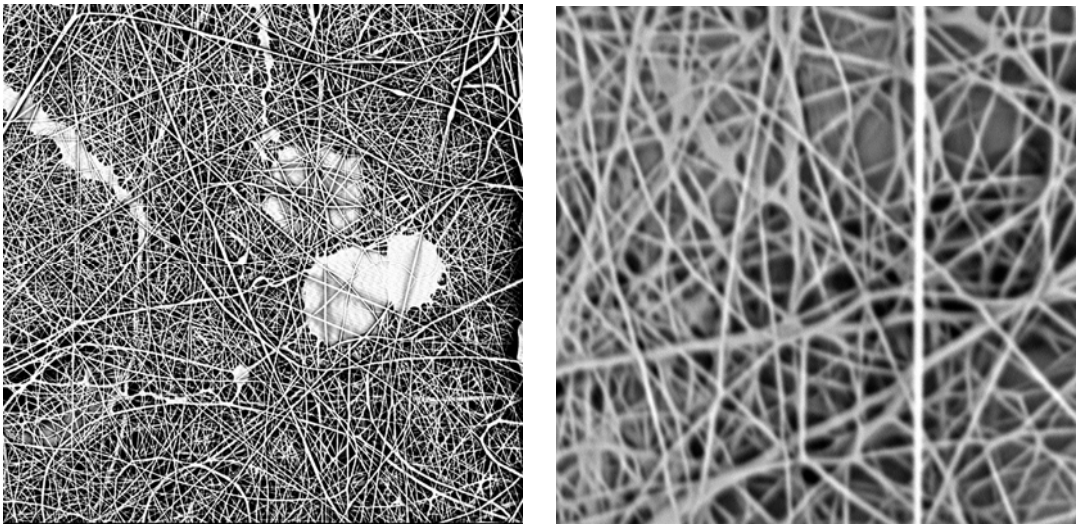

(d) 12%

Figure 8 SEM images of PVA membranes fabricated on PET non-woven substrate by electrospinning of PVA solution at concentrations of (a) 6 wt%; (b) 8 wt%; (c) 10 wt%; (d) 12 wt% at voltage of 32 kV, flow rate of 10 μL/min. Other electrospinning parameters: distance from spinneret to the collector: 10 cm; humidity 55% ± 5%; temperature 24 °C ± 1 °C.

Fig. 8 shows a series of SEM images in order to illustrate the effect of concentration of PVA solutions on the morphological appearance of the electrospun membranes. At a low concentration of 6% or low viscosity of 16 cp, only a few nanofibers were produced, and a large number of microdroplets were formed creating a porous film-like structure. This is because at such low viscosities, the viscoelastic force (a result of the low degree of chain entanglements) in a given jet segment was not large enough to counter the higher Coulumbic force, resulting in the break-up of the charged jet stream, Many studies have reported that a minimum concentration of polymer solution is required for smooth fiber formation [26, 42, 51, 52]. As the concentration was increased to 8% and 10%, beads gradually became less and were eliminated at 10%, whereby a uniform fiber-structure with the fiber diameter of 100 nm was formed. With a further increase in concentration to 12%, beads were formed again in the structure, and the fiber diameter increased to 150 nm. This finding can be explained based on the following argument. When the viscosity was high to 669 cp, the electrical force was not sufficient to fully stretch the fiber due mainly to the high viscoelastic force, resulting in fibers with larger diameter or even beads in the final structure.

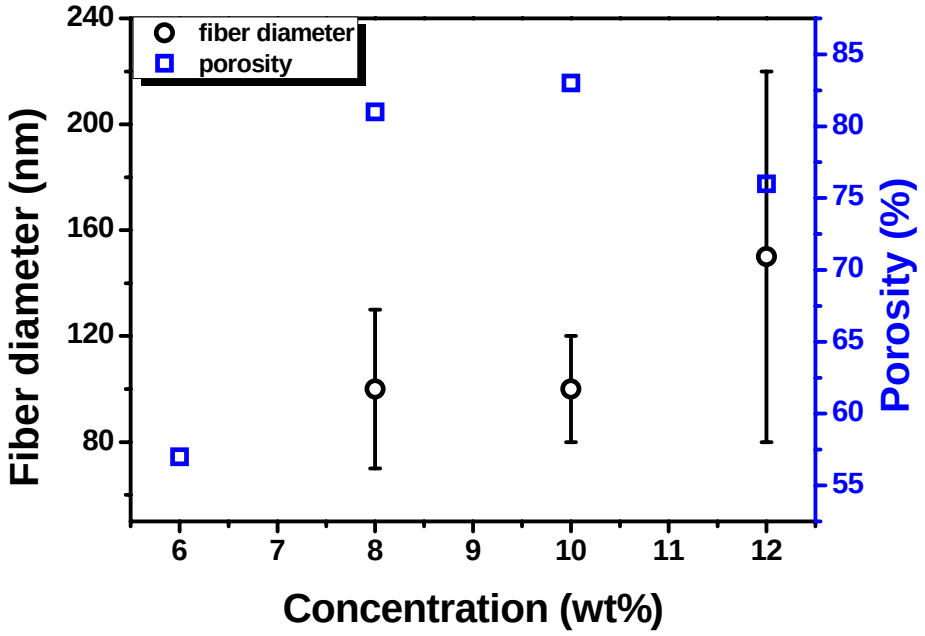

Figure 9 Effects of concentration on fiber diameter and porosity of electrospun PVA membrane.

Table 3 Relationships between viscosity, fiber diameter and porosity at different PVA solution concentrations

PVA concentration	Viscosity (cp)	Fiber diameter (nm)	Porosity
6%	16	-	57%
8%	22	100 ± 30	81%
10%	50	100 ± 20	83%
12%	669	150 ± 70	76%

The porosity of electrospun PVA membranes fabricated by using different PVA concentrations was measured, as listed in Table 3. It is noted that the porosity of the membrane is quite low (57%) because of the film-like structure at the concentration of

6%. Other membranes all exhibited porosity higher than 75%, and the largest one reached to 83% at the 10% concentration.

3.1.3 Effect of ionic salt addition

Adding ionic salt into the PVA solution can change the conductivity of the solution and has a further influence on the morphology of the membrane. It is generally considered that adding salt into the polymer solution can increase the charge density and therefore produce a higher elongation force for the jet stream under the applied electric field, which may result in thinner fibers. However, in Fig. 10, the fiber diameter was found to increase from 100 nm to 160 nm with increasing NaCl contents. This could be due to the higher acceleration at the higher elongation force which reduced the flight time of the jet and shortened the stretching time.

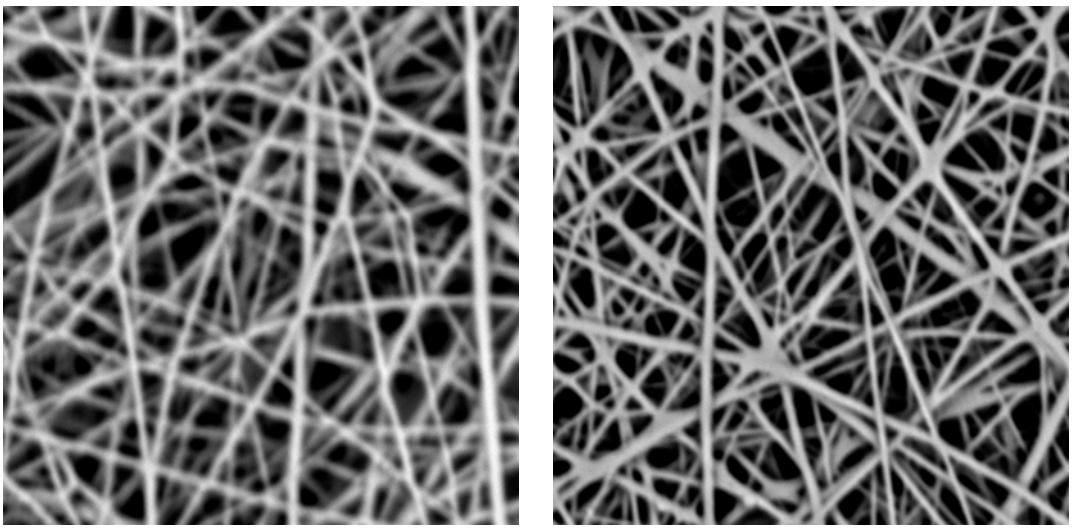

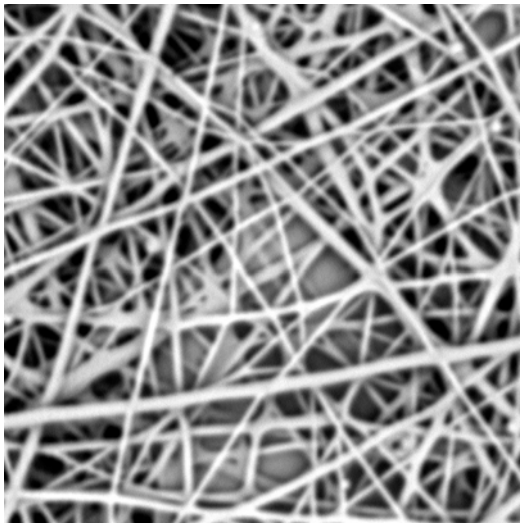

Figure 10 SEM images of PVA membranes fabricated on PET non-woven substrate by electrospinning of a 10 wt% solution at a voltage of 32 kV, flow rate of 10 μL/min, and with NaCl of content (A) 0.1 %; (B) 0.2 %; (C) 0.5%. Other conditions such as humidity and temperature were same as above.

Table 4 Relationship between viscosity, conductivity and e-spun PVA fiber diameter at different NaCl contents

NaCl content (wt %)	**Viscosity (cp)**	**Conductivity (μs/cm)**	**Fiber diameter (nm)**
0	50	312	100 ± 20
0.1	50	933	100 ± 40
0.2	52	1123	120 ± 70
0.5	58	1948	160 ± 70

A careful examination on the viscosities of the solution with different NaCl contents revealed that there was a slight increase in viscosity from 50 cp to 58 cp when the NaCl content was increased from 0.1% to 0.5% as shown in Table 4. The increased viscoelastic force and the shorten flight time were considered to counteract the higher elongation force and be attributed to the increased fiber diameter. Another observation is that the

uniformity of nanofibers decreased as the fiber diameter showed broader distribution with increasing NaCl content. This may be due to the uneven charge distribution in the electrospinning jet.

3.2 Membrane properties evaluation

10% PVA solution without any NaCl added was used for the electrospinning based on the previous experiments, at 32 kV and a flow rate of 10 μL/min as the operating parameters. PVA membranes with five different thicknesses (10 μm, 20 μm, 30 μm, 40 μm and 100 μm) were electrospun onto the PET substrate by delivering different amounts of the polymer solution. Membranes were labeled as M1, M2, M3, M4 and M5 for the convenience of the further discussions. The thickness variation was within 10% for all membranes. Membrane properties were investigated in terms of pure water flux, pore size distribution, and particle rejection ratio. Same tests were also carried out on the Millipore GSWP 0.22 μm microfiltration membrane for comparison.

3.2.1 Pure water flux

Fig. 11 shows the pure water flux of different membranes. It can be seen that at a driven pressure of 2.3 psi, the pure water flux of the electrospun PVA membrane M1 was 10,773 ± 798 L/m^2 h. With increases in the thickness, the pure water flux decreased to 6650 ± 645 L/m^2 h for M2 and gradually to 2,394 ± 266 L/m^2 h for M5. The thicker membrane has a higher hydraulic resistance, partly because of changes related to the effective pore size for such nonwoven structures. Compared with Millipore GSWP 0.22

μm membrane with a pure water flux of 1,048 ± 71 L/m^2 h at 2.3 psi, the electrospun PVA membranes showed much higher flux due to the higher porosity of the electrospun nanofibrous mat.

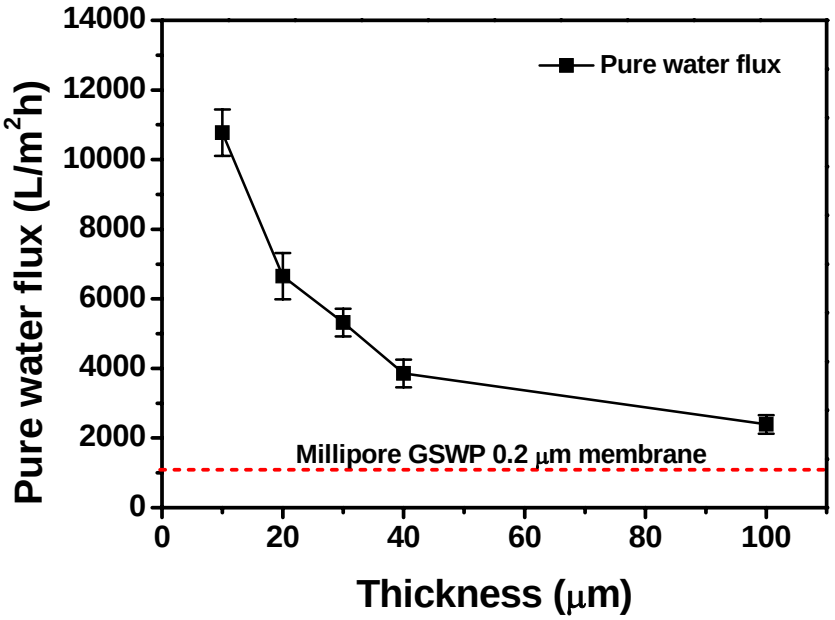

Figure 11 Pure water flux of the Millipore GSWP 0.22 μm membrane and electrospun membranes with different thicknesses

3.2.2 Pore size distribution

Fig. 12 shows typical dry and wet curves of the electrospun PVA membrane M2 obtained from capillary flow porometry. In the wet flow, the starting "bubble point" corresponds to the maximum pore size of the electrospun membrane. The mean flow pressure is the intersection of the half-dry curve with the wet curve, and the mean pore size is calculated with the Young-Laplace equation (Equation 2). As the pressure was increased, the dry and wet curves met at a certain pressure indicating all the pores had been completely "open". Between this point and the "bubble point" was the pore size

range of the electrospun membrane.

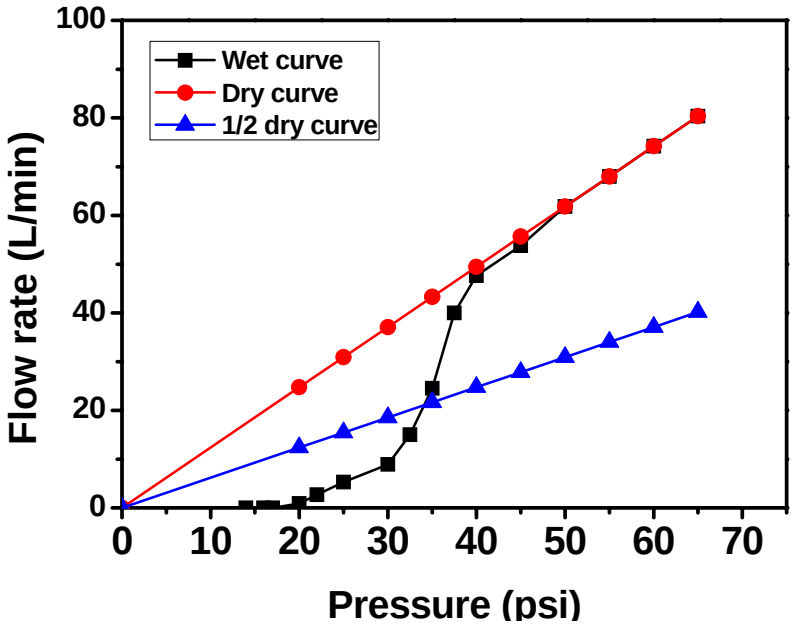

Figure 12 Wet and dry curves of M2 obtained from capillary flow porometry

Fig. 13 shows typical pore size distributions of M1, M2, M3, M4 and M5. For each membrane, the three runs of the capillary flow porometry produced very similar bubble points, and the mean pore sizes varied within 0.01 μm. The only difference among the three runs for each membrane was in the distribution due to the nature of the electrospun membrane. Table 5 summarizes the pore size range and the mean pore size of the electrospun membranes.

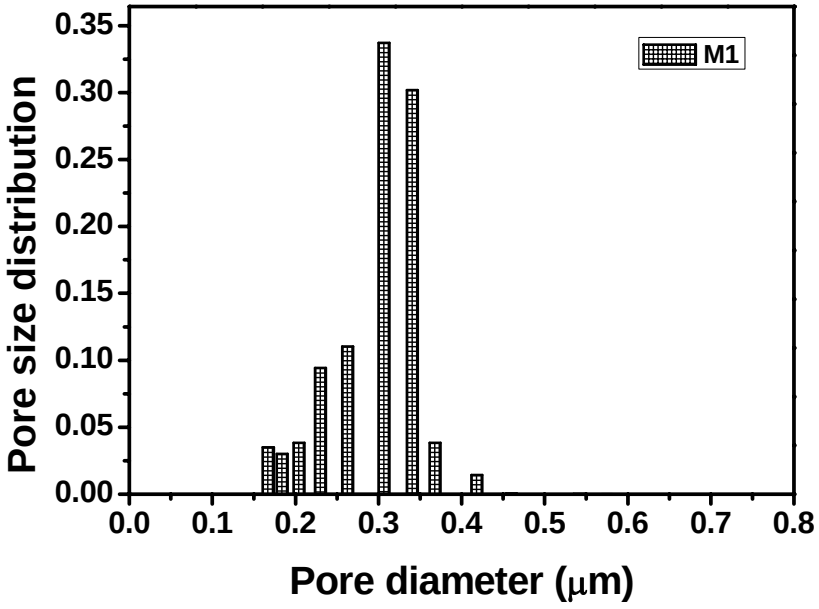
M1
Pore size distribution
0.35
0.30
0.25
0.20
0.15
0.10
0.05
0.00
0.0
0.1
0.2
0.3
0.4
0.5
0.6
0.7
0.8
Pore diameter (μm)

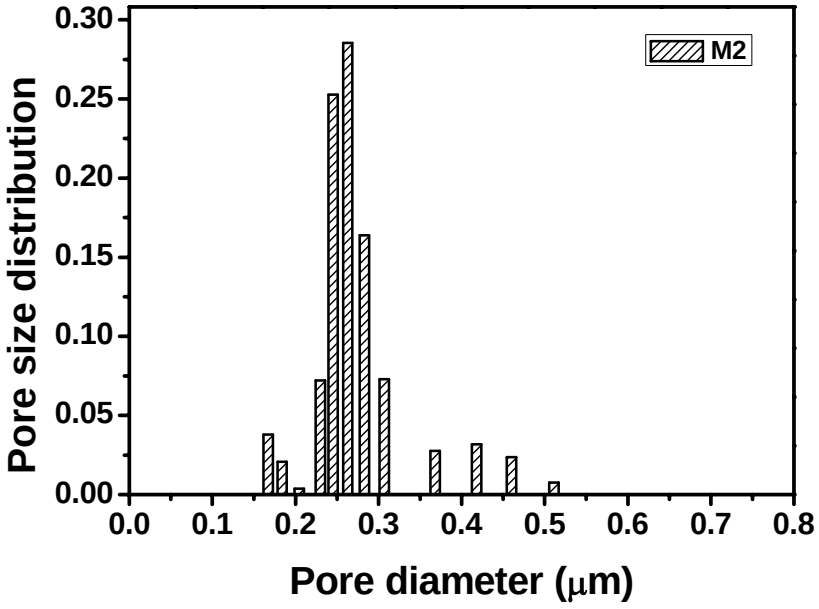
M2
Pore size distribution
0.30
0.25
0.20
0.15
0.10
0.05
0.00
0.0
0.1
0.2
0.3
0.4
0.5
0.6
0.7
0.8
Pore diameter (μm)

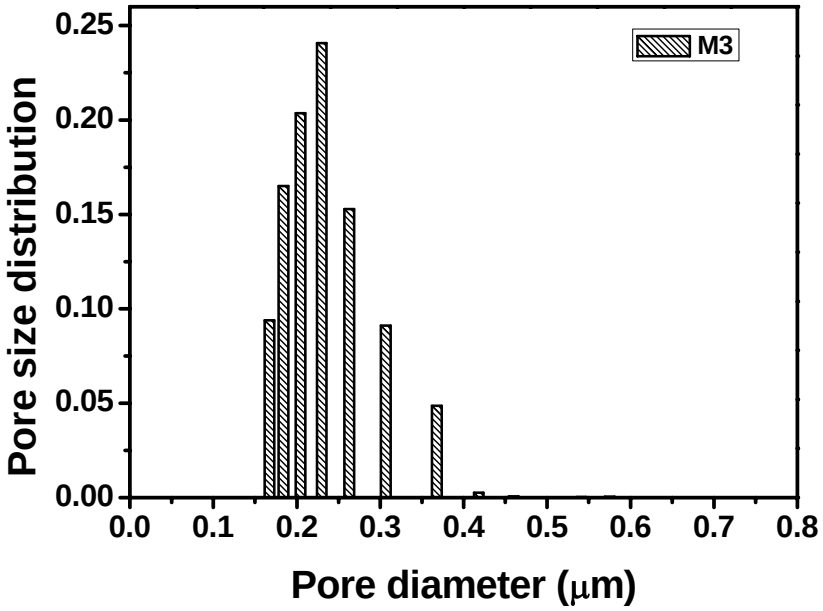
M3
Pore size distribution
0.25
0.20
0.15
0.10
0.05
0.00
0.0
0.1
0.2
0.3
0.4
0.5
0.6
0.7
0.8
Pore diameter (μm)

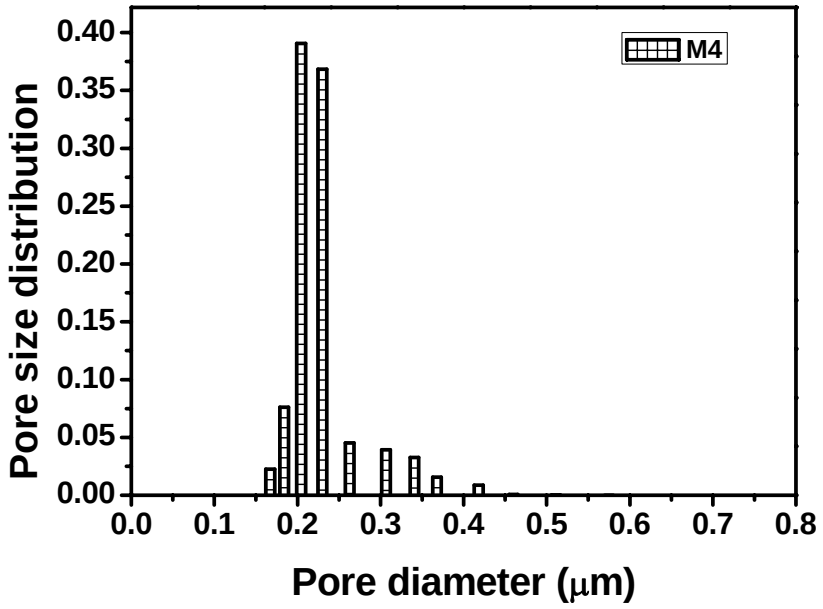
M4
Pore size distribution
0.40
0.35
0.30
0.25
0.20
0.15
0.10
0.05
0.00
0.0
0.1
0.2
0.3
0.4
0.5
0.6
0.7
0.8
Pore diameter (μm)

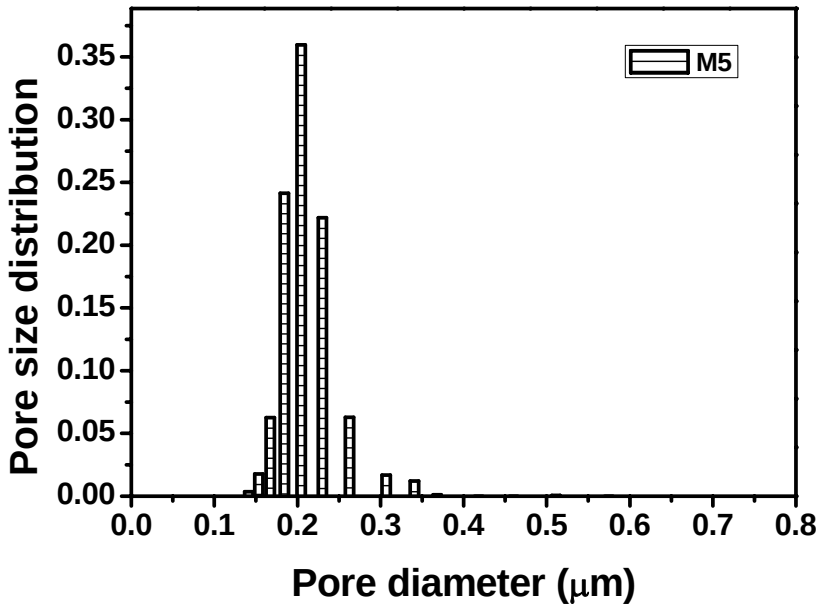

Figure 13 Pore size distribution of electrospun membranes with different thicknesses

Table 5 Pore size range and mean pore size of M 1-5 obtained from capillary flow porometry

Membrane	Pore size range (μm)	Mean Pore size (μm)
M1	0.77~0.17	0.32
M2	0.66~0.17	0.27
M3	0.57~0.17	0.24
M4	0.57~0.17	0.22
M5	0.57~0.15	0.21

From Fig. 13 and Table 5, it can be observed that, for M1 with a thickness of 10 μm, the pore sizes were ranged from 0.77 μm to 0.17 μm, with a mean pore size of 0.32 μm. As the thickness was increased, the maximum pore size was reduced and the pore size range became narrower. For M2 and M3, the pore size range were 0.66 ~ 0.17 μm and

0.57 ~ 0.17 μm, and the mean pore sizes decreased to 0.27 μm and 0.24 μm, respectively. As the electrospun membranes became thicker to 40 μm and 100 μm, the pore size range kept almost unchanged but the pore size distributions shifted slightly towards lower values as shown in Fig. 13.

The effect of the electrospun membrane thickness on the pore size can be explained as follows. Thicker membranes are produced by depositing more fibers on the substrate. As the pores of the electrospun membrane are caused by the entanglement of fibers with other variables (such as fiber diameter and fiber length) being fixed, more fibers crossing a certain area should form smaller pores. This explains why the mean pore size of the electrospun membrane decreased with increasing of the membrane thickness. It should be noted that from the thickness of 40 μm to 100 μm, the mean pore size of the electrospun PVA membrane deceased only by 0.01 μm (or remained essentially the same), from 0.22 μm at a thickness of 40 μm to 0.21 μm at the thickness of 100 μm. This observation indicates that for the electrospun PVA membranes, thickness does not play an important role in reducing the pore size when it has reached ~40 μm and beyond in agreement with results from literature [37].

3.2.3 Particle rejection test

To evaluate the ability of electrospun PVA membranes to function as MF filters, the particle rejection test using 0.209 μm polycarboxylate particles was employed (size deviation of particles was 0.011 μm).

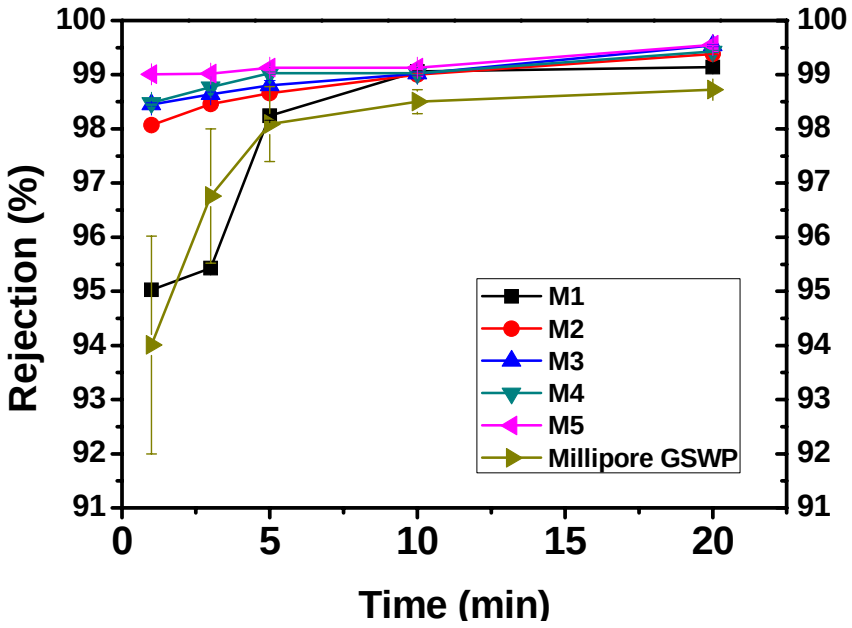

Figure 14 Rejection ratio to 0.2 μm polycarboxylate particles of different membranes vs time

Fig. 14 shows the rejection ratios of different membranes to the particles with time. M 2-5 all exhibited more than 98% of the initial rejection ratios. This finding could not be correlated with previous membrane characterization data which indicated the mean pore sizes of all membranes to be greater than 0.2 μm. To better understand this observation, SEM images were taken on the cross-section, top and bottom surfaces of M2 after the particle rejection test, as shown in Fig. 15. It could be seen in Fig. 15 that the particles were trapped in the top several layers of the electrospun membrane, with no obvious particles within the membrane or at the bottom surface. It should be noted that the particles could easily get into the membrane as most of the pores on the top layer were greater than 0.2 μm. As the particles went deeper, the effective pore size in the flow direction became smaller due to the increasing intersections of the fibers. In another

aspect, the electrospun nanofibers were packed very closely in the cross-section as seen in Fig. 15 (E), and the height of most void space in the cross-section was around 100 nanometer (average diameter of electrospun PVA nanofiber), which was the smaller than the particle size. So there was little chance for the particles to move laterally in the electrospun membrane. Therefore, when the pore size in the flow direction was reduced to less than 0.2 μm within the top few layers, the particles were retained as seen in Fig. 15 (C) and (D).

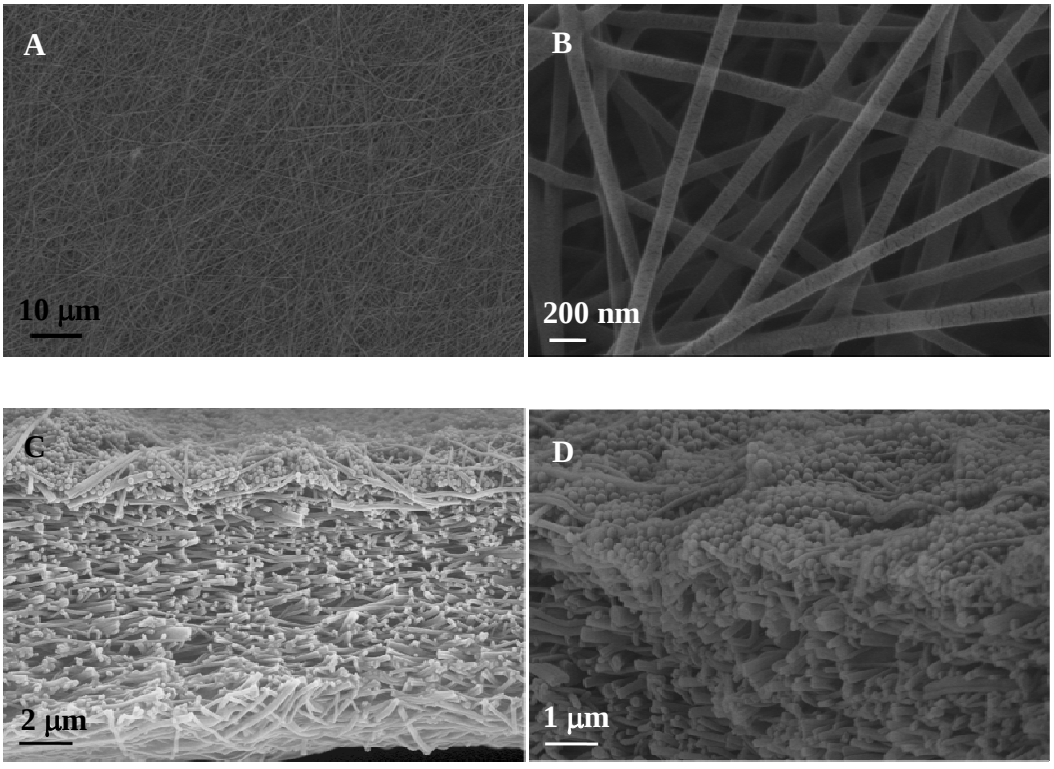

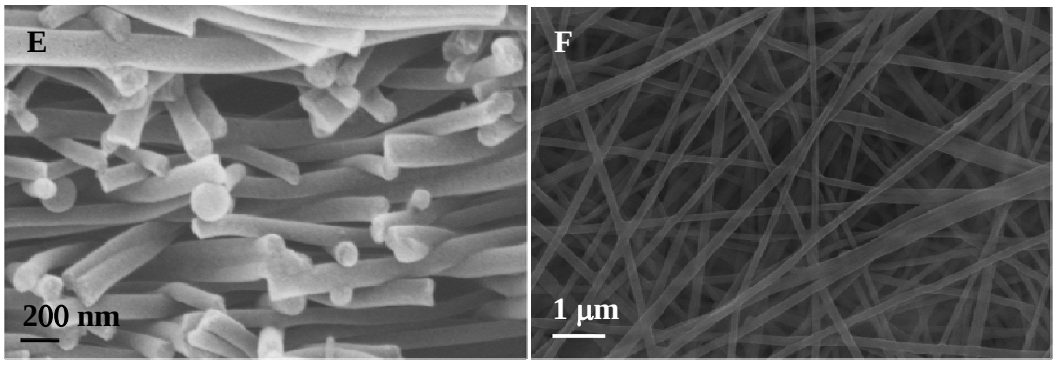

Figure 15 SEM images of electrospun PVA membrane M2. (A) top surface before filtration 3,000 ×, (B) top surface before filtration 100,000 ×, (C) cross-section after the particle rejection test 15,000 ×, (D) top layers of the cross-section after particle rejection test 30,000 ×, (E) middle part of the cross-section after particle rejection test 100,000 ×, (F) bottom surface after the particle rejection test 30,000 ×.

For Millipore GSWP 0.22 μm membrane, it showed 93.78% ± 2.52% rejection to the 0.2 μm polycarboxylate particles. The SEM images of Millipore GSWP membranes before and after particle rejection test are shown in Fig. 16. From the SEM images it can be seen that the Millipore GSWP membrane has relatively large pores in all dimensions, which makes it easier to be filled up with small particles. As a result, after the rejection test the whole membrane had been fouled even on the bottom surface, as shown in Fig. 16 (C). As a result, there were more particles penetrating through the membrane, resulting in a lower rejection ratio than the electrospun membranes.

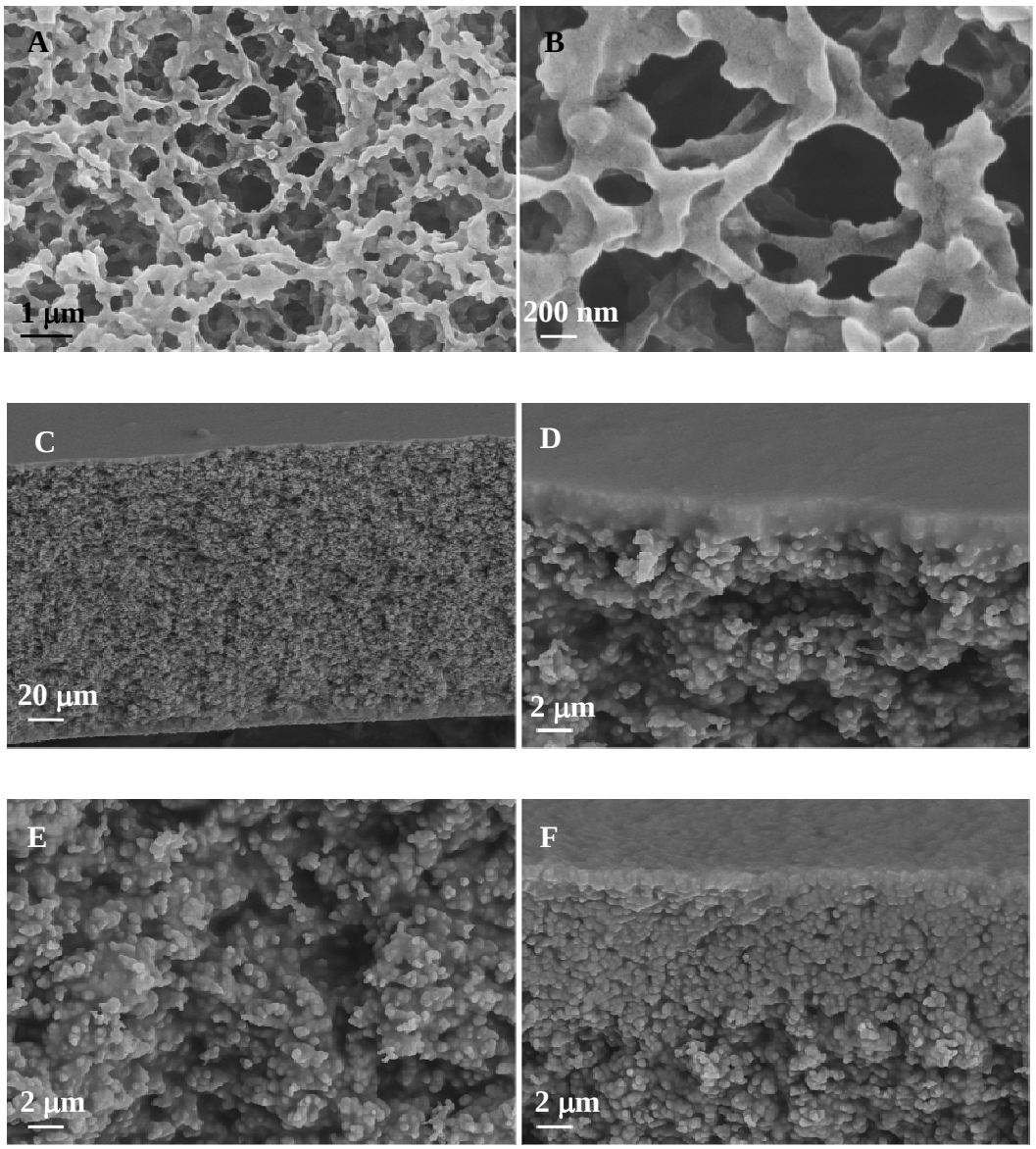

Figure 16 SEM images of Millipore GSWP 0.22 μm membrane M2. (A) top surface before filtration 30,000 ×, (B) top surface before filtration 100,000 ×, (C) cross-section after the particle rejection test 1,000 ×, (D) top part of cross-section after the particle rejection test 10,000 ×, (E) middle part of cross-section after the particle rejection test 10,000 ×, (F) bottom part of cross-section after the particle rejection test 10,000 ×.

For all membranes, the rejection ratio was increased and the permeate flux dropped sharply as shown in Fig. 17 because in the rejection test and with increasing time, more and more particles were deposited on the membrane and formed a layer which reduced

the effective pore size of the electrospun membranes and the permeate flux. Overall, the electrospun membranes exhibited a much higher permeate flux than the Millipore GSWP membrane, because the electrospun membranes could still hold high porosity in the "screen filter" layer even if there was a "cake layer" formed on the top.

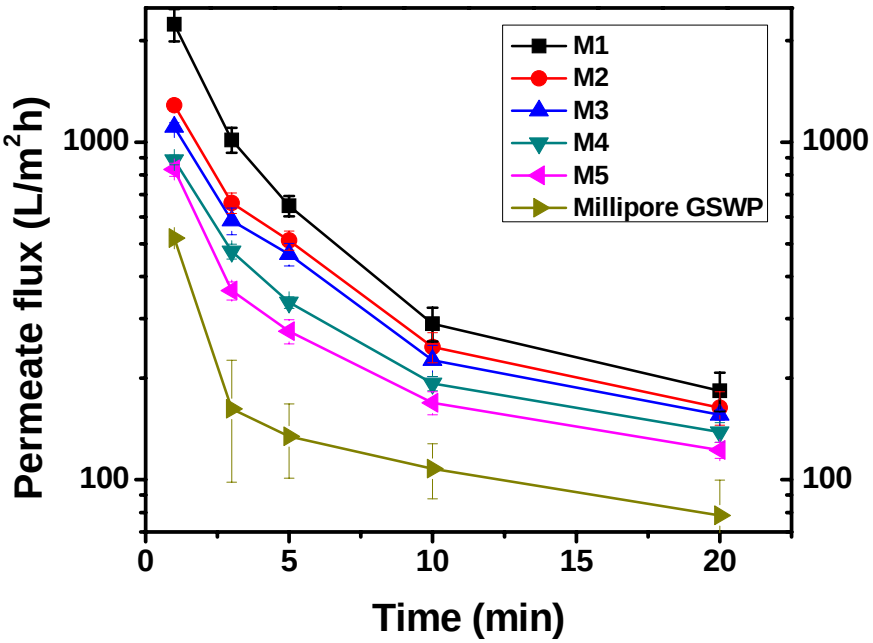

Figure 17 Permeate flux of different membranes in the rejection test vs time.

4. Conclusions

The electrospinning technique was used to fabricate nanofibrous membranes for microfiltration applications in this study. The effects of processing voltage and solution properties including concentration and ionic salt addition were thoroughly investigated. Results demonstrated that at a high voltage of 32 kV, the spinneret-to-collector distance of 10 cm, and the PVA solution concentration of 10 wt%, the formation of uniform

nanofibers with no beads can be achieved. The diameter of the nanofibers was found to increase with the addition of NaCl. Electrospun membranes with a fiber diameter of 100 nm were fabricated into the thicknesses of 10 μm, 20 μm, 30 μm, 40 μm and 100 μm. Filtration membrane properties, such as the pore size distribution and the mean pore size, pure water flux and rejection to the 0.2 μm polycarboxylate particles, were investigated. Same properties of the Millipore GSWP 0.22 μm membrane were also tested for comparison. It was shown that the mean pore size was decreased with the membrane thickness below 30 μm and could be kept almost the same when the thickness reached 40 μm and beyond. Pure water flux of the electrospun membranes monotonically decreased with increasing thickness. Based on membrane thickness, these membranes showed 2.5 to 9 times higher pure water flux than the comparable Millipore membrane. Rejection test revealed that the membranes with a thickness of 20 μm or more could reject more than 98 % of the 0.2 μm polycarboxylate particles, which was higher than the rejection ratio of the Millipore GSWP membrane. Despite the “cake layer” formation during the rejection test, the electrospun membranes could still be kept at a higher permeate flux than the Millipore GSWP membrane, possibly due to the high porosity of the ‘unfouled’ screen filter layer. Considering the filtration performance and the production cost, the electrospun membrane with a thickness of ~20 μm should be a good candidate for the novel filtration membrane, as it demonstrated more than 5 times pure water flux, 2 ~ 4 times permeate flux in the rejection test with a 98 % rejection ratio to the 0.2 μm particles. With proper module design, there would be a potential for the electrospun PVA

membranes to be used to remove the bacteria in surface water effectively. There is also potential of using these electrospun membranes as the pre-filter prior to ultrafitration or nanofiltration to minimize the possibility of fouling and contamination from micro-organisms or microparticles.

List of References

1. Kosek M, Bern C, and Guerrant RL. Bulletin of the World Health Organization 2003;81(3):197-204.
2. Wang YY, Hammes F, Duggelin M, and Egli T. Environmental Science & Technology 2008;42(17):6749-6754.
3. Knight SM, Toodayan W, Caique WC, Kyi W, Barnes A, and Desmarchelier P. International Journal of Epidemiology 1992;21(4):812-818.
4. Huq A, Xu B, Chowdhury MAR, Islam MS, Montilla R, and Colwell RR. Applied and Environmental Microbiology 1996;62(7):2508-2512.
5. Reller ME, Mendoza CE, Lopez MB, Alvarez M, Hoekstra RM, Olson CA, Baier KG, Keswick BH, and Luby SP. American Journal of Tropical Medicine and Hygiene 2003;69(4):411-419.
6. Van der Bruggen B, Everaert K, Wilms D, and Vandecasteele C. Journal of Membrane Science 2001;193(2):239-248.
7. Thanuttamavong M, Yamamoto K, Oh JI, Choo KH, and Choi SJ. Desalination 2002;150(2):209-210.
8. Gewin V. Nature 2005;436(7048):173-173.
9. Gullinkala T and Escobar I. Environmental Progress 2008;27(2):210-217.
10. Farahbakhsh K, Svrcek C, Guest RK, and Smith DW. Journal of Environmental Engineering and Science 2004;3(4):237-253.

11. Van der Bruggen B, Vandecasteele C, Van Gestel T, Doyen W, and Leysen R. Environmental Progress 2003;22(1):46-56.

12. Yoon K, Kim K, Wang XF, Fang DF, Hsiao BS, and Chu B. Polymer 2006;47(7):2434-2441.

13. Mchugh AJ and Miller DC. Journal of Membrane Science 1995;105(1-2):121-136.

14. Zhang SH, Jian XG, and Dai Y. Journal of Membrane Science 2005;246(2):121-126.

15. Lin DJ, Chang CL, Chen TC, and Cheng LP. Desalination 2002;145(1-3):25-29.

16. Kim IC, Yoon HG, and Lee KH. Journal of Applied Polymer Science 2002;84(6):1300-1307.

17. KastelanKunst L, Dananic V, Kunst B, and Kosutic K. Journal of Membrane Science 1996;109(2):223-230.

18. Boussu K, Vandecasteele C, and Van der Bruggen B. Polymer 2006;47(10):3464-3476.

19. Paulsen FG, Shojaie SS, and Krantz WB. Journal of Membrane Science 1994;91(3):265-282.

20. Wang XF, Fang DF, Yoon K, Hsiao BS, and Chu B. Journal of Membrane Science 2006;278(1-2):261-268.

21. Akthakul A, McDonald WF, and Mayes AM. Journal of Membrane Science 2002;208(1-2):147-155.

22. Nakao S. Journal of Membrane Science 1994;96(1-2):131-165.

23. Marshall AD, Munro PA, and Tragardh G. Desalination 1993;91(1):65-108.

24. Deitzel JM, Kosik W, McKnight SH, Tan NCB, DeSimone JM, and Crette S. Polymer 2002;43(3):1025-1029.

25. Seeram Ramakrishna KF, Wee-Eong Teo, Teik-Cheng Lim, Zuwei Ma. An introduction to Electrospinning and Nanofibers, 2005.

26. Lin K, Chua KN, Christopherson GT, Lim S, and Mao HQ. Polymer 2007;48(21):6384-6394.

27. Tripatanasuwan S, Zhong ZX, and Reneker DH. Polymer 2007;48(19):5742-5746.

28. Li D and Xia YN. Advanced Materials 2004;16(14):1151-1170.

29. Fridrikh SV, Yu JH, Brenner MP, and Rutledge GC. Physical Review Letters 2003;90(14):-.

30. Demir MM, Yilgor I, Yilgor E, and Erman B. Polymer 2002;43(11):3303-3309.

31. Matthews JA, Wnek GE, Simpson DG, and Bowlin GL. Biomacromolecules 2002;3(2):232-238.

32. Hajra MG, Mehta K, and Chase GG. Separation and Purification Technology 2003;30(1):79-88.

33. Min BM, Lee G, Kim SH, Nam YS, Lee TS, and Park WH. Biomaterials 2004;25(7-8):1289-1297.

34. Wang A, Singh H, Hatton TA, and Rutledge GC. Polymer

2004;45(16):5505-5514.

35. Wang XF, Chen XM, Yoon K, Fang DF, Hsiao BS, and Chu B. Environmental Science & Technology 2005;39(19):7684-7691.

36. Jin HJ, Fridrikh SV, Rutledge GC, and Kaplan DL. Biomacromolecules 2002;3(6):1233-1239.

37. Li DP, Frey MW, and Joo YL. Journal of Membrane Science 2006;286(1-2):104-114.

38. Ryu YJ, Kim HY, Lee KH, Park HC, and Lee DR. European Polymer Journal 2003;39(9):1883-1889.

39. Doshi J and Reneker DH. Journal of Electrostatics 1995;35(2-3):151-160.

40. Baumgart.Pk. Journal of Colloid and Interface Science 1971;36(1):71-&.

41. Fong H, Chun I, and Reneker DH. Polymer 1999;40(16):4585-4592.

42. Megelski S, Stephens JS, Chase DB, and Rabolt JF. Macromolecules 2002;35(22):8456-8466.

43. Bognitzki M, Czado W, Frese T, Schaper A, Hellwig M, Steinhart M, Greiner A, and Wendorff JH. Advanced Materials 2001;13(1):70-+.

44. Dai WS and Barbari TA. Journal of Membrane Science 1999;156(1):67-79.

45. Ding B, Kim HY, Lee SC, Shao CL, Lee DR, Park SJ, Kwag GB, and Choi KJ. Journal of Polymer Science Part B-Polymer Physics 2002;40(13):1261-1268.

46. Gopal R, Kaur S, Ma ZW, Chan C, Ramakrishna S, and Matsuura T. Journal of Membrane Science 2006;281(1-2):581-586.

47. Hernandez A, Calvo JI, Pradanos P, and Tejerina F. Journal of Membrane Science 1996;112(1):1-12.

48. Mcguire KS, Lawson KW, and Lloyd DR. Journal of Membrane Science 1995;99(2):127-137.

49. Tomihata K and Ikada Y. Journal of Polymer Science Part a-Polymer Chemistry 1997;35(16):3553-3559.

50. Jena A and Gupta K. American Ceramic Society Bulletin 2005;84(3):28-30.

51. Buchko CJ, Chen LC, Shen Y, and Martin DC. Polymer 1999;40(26):7397-7407.

52. Shenoy SL, Bates WD, Frisch HL, and Wnek GE. Polymer 2005;46(10):3372-3384.